LAWRENCE
LIVERMORE
NATIONAL
LABORATORY

LLNL-CONF-479976

ELECTRICAL CONDUCTIVITY OF LABORATORY-SYNTHESIZED METHANE HYDRATE

W. L. Du Frane, L. A. Stern, K. A. Weitemeyer, S. Constable, J. C. Pinkston, J. J. Roberts

April 11, 2011

International Conference on Gas Hydrates 7
Edinburgh, Ireland
July 17, 2011 through July 21, 2011

Disclaimer

Proceedings of the 7th International Conference on Gas Hydrates (ICGH 2011),
Edinburgh, Scotland, United Kingdom, July 17-21, 2011.

ELECTRICAL CONDUCTIVITY OF LABORATORY-SYNTHESIZED METHANE HYDRATE

Wyatt L. Du Frane[1,*], Laura A. Stern[2], Karen A. Weitemeyer[3], Steven Constable[3], John C. Pinkston[2], Jeffery J. Roberts[1]

[1]Lawrence Livermore National Laboratory
7000 East Ave
Livermore, CA 94551
UNITED STATES OF AMERICA

[2]U. S. Geological Survey
345 Middlefield Rd, MS/977
Menlo Park, CA 94025
UNITED STATES OF AMERICA

[3]Scripps Institution of Oceanography
8800 Biological Grade
La Jolla, CA 92093
UNITED STATES OF AMERICA

ABSTRACT

Electromagnetic (EM) remote-sensing techniques are demonstrated to be sensitive to gas hydrate concentration and distribution and complement other resource assessment techniques, particularly seismic methods. To fully utilize EM results requires knowledge of the electrical properties of individual phases and mixing relations, but little is known about the electrical properties of gas hydrates. We developed a pressure cell to synthesize gas hydrate while simultaneously measuring in situ frequency-dependent electrical conductivity (σ). Synthesis of methane (CH_4) hydrate was verified by thermal monitoring and by post run cryogenic scanning electron microscopy (cryo-SEM). Cryo-SEM was also used to examine the distribution of a CH_4 hydrate-quartz sand mixture. The cell was tested by collecting impedance (Z) spectra (20 Hz to 2 MHz) on solid ice, Teflon, and parallel resistor-capacitor (R-C) circuits. Z spectra were collected before and after synthesis of polycrystalline CH_4 hydrate from polycrystalline ice and used to calculate σ. We determined the σ of CH_4 hydrate to be 5 x 10^{-5} S/m at 0 °C with activation energy (E_a) of 30.6 kJ/mol (-15 to 15 °C). After dissociation back into ice, σ measurements of samples increased by a factor of ~4 and E_a increased by ~50%, similar to the starting ice samples.

Keywords: gas hydrates, electrical conductivity, methane

NOMENCLATURE

Cryo Cryogenic
DDI Distilled-deionized
E_a Activation energy (kJ/mol)
EM Electromagnetic
LCR Inductance-capacitance-resistance
ppm Parts per million by weight
R-C Parallel resistor (Ω)–capacitor (pF)
SEM scanning electron microscopy
Z Impedance (Ω)
σ Electrical conductivity (S/m)
σ_0 Pre-exponential term (S/m)

[*] Corresponding author: Phone: 1-925-423-8026 Email: dufrane2@llnl.gov

INTRODUCTION

Clathrate hydrates of natural gas are compounds with an ice-like crystalline framework that encages guest gas molecules, most commonly methane (CH_4). CH_4 hydrate formation requires cool temperature, high pressure, and sufficient supplies of H_2O and CH_4; these conditions are met in both marine and permafrost regions worldwide [1]. CH_4 hydrate is potentially a significant source of clean, low-carbon energy. However, much of the naturally occurring hydrate in the arctic exists at the edge of thermodynamic stability posing an environmental hazard that threatens release of potent greenhouse [e.g., 2; See review in 3]. Gas hydrate instability has been associated with some of the largest marine landslides documented in the geologic record [4, 5], and poses a more local and immediate threat to drilling and wellbore stability [6-8].

CH_4 hydrate occurs in vast quantities, with an estimate of 10,000 Gt of CH_4 as the highly cited 'consensus value' [1, 9]; however, other estimates span several orders of magnitude as a result of continued efforts at direct and indirect observation and by the development of more complex global models [3, 10-12]. Current geophysical surveying methods for identifying hydrate are limited. Well logging or coring is expensive, invasive, and provides only a point measurement for the direct presence of hydrate. Seismic methods detect hydrate using seismic bottom simulating reflectors, blanking, and bright spots [e.g., 13]. Quantifying the volume fraction of hydrate in sediments may be possible with careful processing and inversion of seismic data [e.g., 13-16], but this approach is complicated.

Well logging indicates that regions containing hydrate are significantly less conductive than water saturated zones [e.g., 17]. This is consistent with the demonstrated sensitivity of electromagnetic (EM) methods to the concentration and geometric distribution of hydrate and pore fluid [18-22]. However, to make quantitative estimates of hydrate volume using EM methods requires knowledge of the electrical conductivity (σ) of gas hydrates in combination with petrophysical mixing relations, particularly in cases of highly saturated gas hydrate with only poorly connected pore water.

Gas hydrates have similar chemical bonding to ice, which suggests a similar point defect structure may determine electrical properties. The electrical properties of ice have been studied extensively, and inferences can be drawn from this work as to what charge carrying defects exist in gas hydrates. Typically for ice and hydrate crystal structures, each oxygen atom is bonded with two shared hydrogen atoms. In ice, charge is conducted by defects that violate this rule. There are intrinsic and extrinsic defects, and their contributions to σ have separate temperature dependences [e.g., 23]. The intrinsic defects in ice are Bjerrum defects (i.e. rotational faults), where an H_2O molecule has rotated to cause two hydrogens to occupy the space between neighboring oxygens (D-defect) and/or zero hydrogens to occupy the space between neighboring oxygens (L-defect) [e.g., 23]. The extrinsic defects in ice are protonic defects, such as an oxygen atom bonded with three hydrogen atoms - H_3O^+ or bonded with one hydrogen atom – OH^-. Although chemical impurities (such as NaCl) are largely excluded during the formation of ice and gas hydrates from seawater, quantities as low as several ppm are accommodated by intrinsic and extrinsic defects [e.g., 23]. Therefore the σ of ice is highly dependent on the type and concentration of impurities present. Also there are higher concentrations/mobilities of defects in grain surfaces where it takes less energy to form than within the bulk grains [e.g., 23]. Charge is likely conducted in gas hydrates by similar defects, in which case σ may depend on impurities and grain size similar to ice.

To date, there have been few published measurements on the electrical properties of sediment-gas hydrate-water mixtures and none on unmixed, single-phase CH_4 hydrate. Gas hydrate is less conductive compared to water with ionic impurity [17], and this knowledge has been used to verify gas hydrate formation and decomposition in experiments [24]. Spangenberg and Kulenkampff [25] examined the σ of glass beads as a function of CH_4 hydrate saturation in the pore space at ~13 °C. Lee et al. [26] published a systematic examination of σ and permittivity results for tetrahydrofuran hydrate (an analog for natural gas hydrate) mixed with sand, silts, and clay at ~ 0 °C. Ren et al. [27] studied a mixture of quartz sand-CH_4 hydrate-

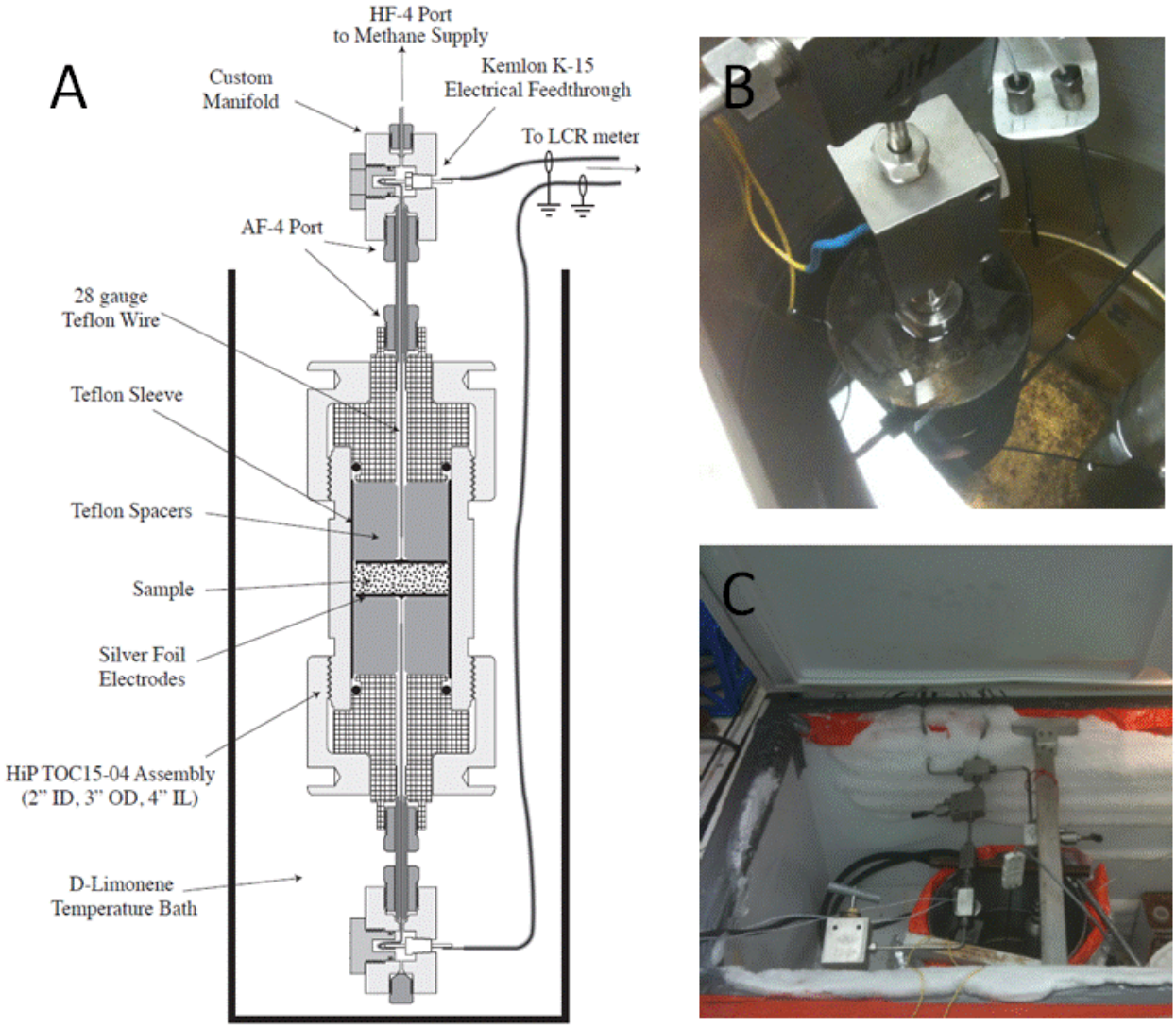

Figure 1 A) Schematic of pressure cell for CH_4 hydrate synthesis with in situ σ measurement (from Du Frane et al., *In Press, Geophys. Res. Lett.*). B) Pressure cell inside of a D-limonene temperature bath, with CH_4 reservoir. C) D-limonene temperature bath and pressure plumbing above heater inside a chest freezer.

seawater from 5-30 °C, however temperature was not controlled independently of CH_4 hydrate saturation. These previous studies on mixed samples help resolve mixing laws, but are dominated by the water and/or sedimentary phases, with no quantitative information on the σ of gas hydrate. In this study we present the first σ measurements on CH_4 hydrate that is unmixed (fully reacted), porous, polycrystalline over a temperature range that encompasses that of natural hydrate formations.

EXPERIMENTAL TECHNIQUES

We designed a specialty pressure cell to form polycrystalline CH_4 hydrate for in situ impedance (Z) measurements (Figure 1A). The cell is built around a commercially available double-ended pressure vessel manufactured by High Pressure Equipment Co. with a pressure rating of 5,000 psi (34.5 MPa). Silver foil electrodes are connected by Teflon insulated wire to high pressure electrical feedthroughs (Kemlon brand K-15) on the inner (high pressure) side and an Agilent E4980A LCR (inductance-capacitance-resistance) meter on the

Table 1 Summary of experimental conditions and Equation 1 fit parameters σ_0 and E_a (modified from Du Frane et al., *In Press, Geophys. Res. Lett.*).

Run	Sample condition	Heating Cycle	Heating Rate (°C/hr)	Pore CH_4 Pressure (MPa)	Log(σ_0 (S/m))	E_a (kJ/mol)
-	Solid Ice Test	1	1.3	0	2.62*	37.5*
1	Synthesis Test	n/a	6.2	16.9-25.8†	n/a	n/a
2	Ice w/ CH_4	1	7.4	21.7-26.2	1.16*	25.8*
	CH_4 hydrate	11	5.9	18.3-21.3	0.965	27.9
	Dissociated to ice	12	4.7	0	6.63*	54.5*
3	Ice w/ CH_4	1	9.8	23.0-26.7	0.376*	21.8*
	CH_4 hydrate	7	Step-Dwell	16.2-18.5	1.50	30.6
	Dissociated to ice	8	Step-Dwell	0	5.00*	45.3*
4	~50:50 vol% CH_4 Hydrate:Sand	n/a	8.0	22.5-29.0†	n/a	n/a

†Pressure range over entire run.
*Fits only include data below ice melting point.

outer side. The cell encloses a 5 x 1.25-cm disc-shaped sample, with electrodes at each end and capped by Teflon spacers and surrounded by a Teflon sleeve.

The Agilent LCR meter was used to measure complex Z spectra between 20 Hz to 2 MHz with a relative accuracy 0.01% degrading to 1% for Z of 10 MΩ. The assembly was tested for electrical leakage using a blank sample made of Teflon, ice frozen from reagent grade water, and a variety of parallel resistor-capacitor (R-C) circuits (10-316 kΩ; 1.15-22 pF). We then performed 4 runs with CH_4 hydrate: run 1 with a thermocouple installed in the cell to verify the synthesis process and extent of reaction, runs 2 and 3 to measure σ, run 4 to synthesize a uniform phase distribution of a methane hydrate + sand sample.

Samples of CH_4 hydrate were synthesized from a granular ice + CH_4 gas mixture at 25 +/- 5 MPa using a temperature cycling method described previously in Stern et al. [28, 29]. The pressure vessel sits in a D-limonene temperature bath above a heater, both in a chest freezer maintained at ~-15 °C (Figure 1B and 1C). The reactant ice was made from a block of nearly gas-free ice grown from distilled-deionized (DDI) water, then crushed and sieved to 180-250 μm. We measured Z and σ in runs 2 and 3 during the first heating cycle, after full reaction to CH_4 hydrate, and after samples were dissociated back into polycrystalline ice. Heating was isochoric such that the pore pressure of CH_4 gas increased during the measurement (pressure ranges are listed in Table 1). While heating or cooling, temperature in the center of the run 1 sample lagged slightly behind bath temperature by 1-5°C, leading to slight uncertainty in sample temperature during heating for runs 2 and 3. We addressed this in run 3 by monitoring Z at a single frequency after each heating increment and recording σ after it stopped changing. In Table 1 this is called 'step-dwell'.

Cryogenic scanning electron microscopy (cryo-SEM) was used to observe the grain size and appearance of the final CH_4 hydrate formed in run 1. For this procedure the vessel was cooled sufficiently with liquid nitrogen prior to depressurization and opening of the cell. A thermocouple embedded in the sample was used to ensure stability of the hydrate during the quenching procedure, recovery, and transfer to the cryo-preparation station (Gatan Alto Model 2100). The sample was cleaved under vacuum in the preparation station to produce fresh surfaces uncontaminated by water condensation, and then transferred under vacuum to a LEO982 field emission SEM. A thermocouple embedded in the SEM sample stage monitored temperature throughout the imaging process. Imaging was conducted at temperature < -185 °C, vacuum $<10^{-6}$ kPa, and accelerating voltage of 2 kV. Further details are given in Stern et al. [29].

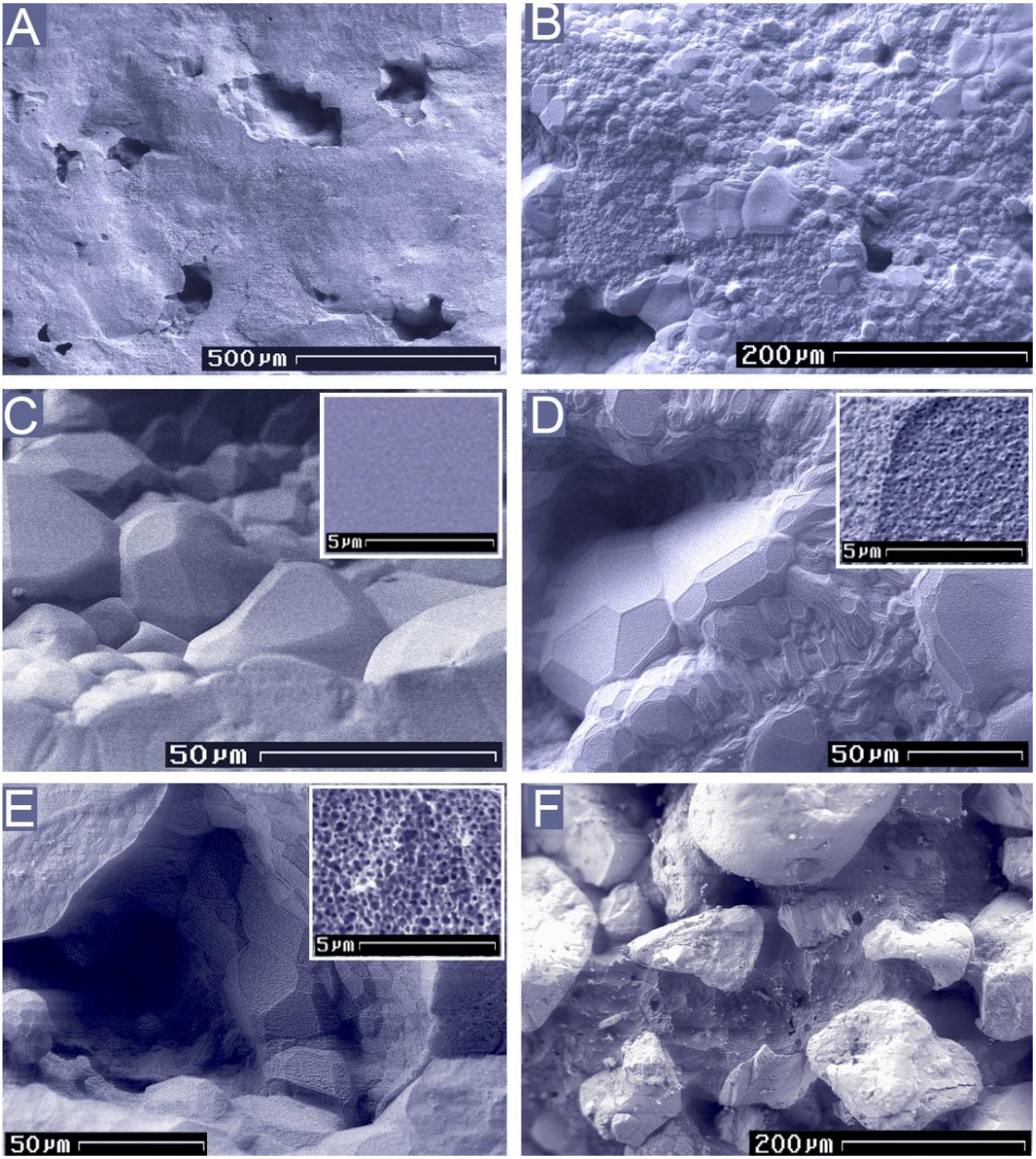

Figure 2 Cryo-SEM images of samples formed in runs 1 and 4 at varying magnifications (modified from Du Frane et al., *In Press, Geophys. Res. Lett.*). The overall sample appearance and unconnected nature of the pore space in single-phase, unmixed CH_4 hydrate from run 1 is shown in A and B. This sample has ~ 20-70 µm average grain diameters and ~ 20% intergranular porosity. Images C, D, and E were taken 20 minutes apart with closer views of individual grains with inset views of detailed grain surface topology. Individual hydrate grains are fully dense after removal from the sample chamber and upon first inspection (C and C inset), but undergo sublimation and surface degradation within 20 minutes in the FE-SEM high vacuum conditions, developing a nano- to meso-porous structure (D and E insets). Image F shows the run 4 sample, in which CH_4 hydrate (appears as the darker-colored connecting material between the sand grains) and OK#1 quartz sand grains (appear light in color and stand high in relief due to partial sublimation of the CH_4 hydrate) each occupy ~50 vol. % of the solid material here.

RESULTS

Cryo-SEM images of the crystal morphology and thermal monitoring of run 1 confirmed the synthesis of CH_4 hydrate (Figure 2). The resulting polycrystalline material has 20 – 70 µm average grain diameters and ~ 20% intergranular porosity (i.e. 80% dense). The porosity is also known independently from mass measurements of the reactant ice prior to loading the cell. Most of the porosity occurs as isolated and virtually unconnected cavities (Figure 2a). Ice was not observed in the interior of the sample. Images of run 4 indicate that CH_4 hydrate and quartz sand (OK#1) grains were evenly distributed throughout the sample (Figure 2f).

Plots of complex Z spectra of samples from run 2 and run 3 consist of two overlapping semicircular arcs (Figure 3). The silver foil electrodes are polarizing and did not allow transfer of charge from the samples and electrodes (i.e., 'blocking'), resulting in large low frequency arcs (partially shown in Figure 3). The smaller high frequency arcs are attributed to sample properties [30]. Z spectra were fit with an equivalent circuit of two R-Cs in series [31], which demonstrated that σ could be reliably measured with the frequency associated with the smallest phase angle to eliminate electrical response related to the vessel, leads or electrodes (Figure 3).

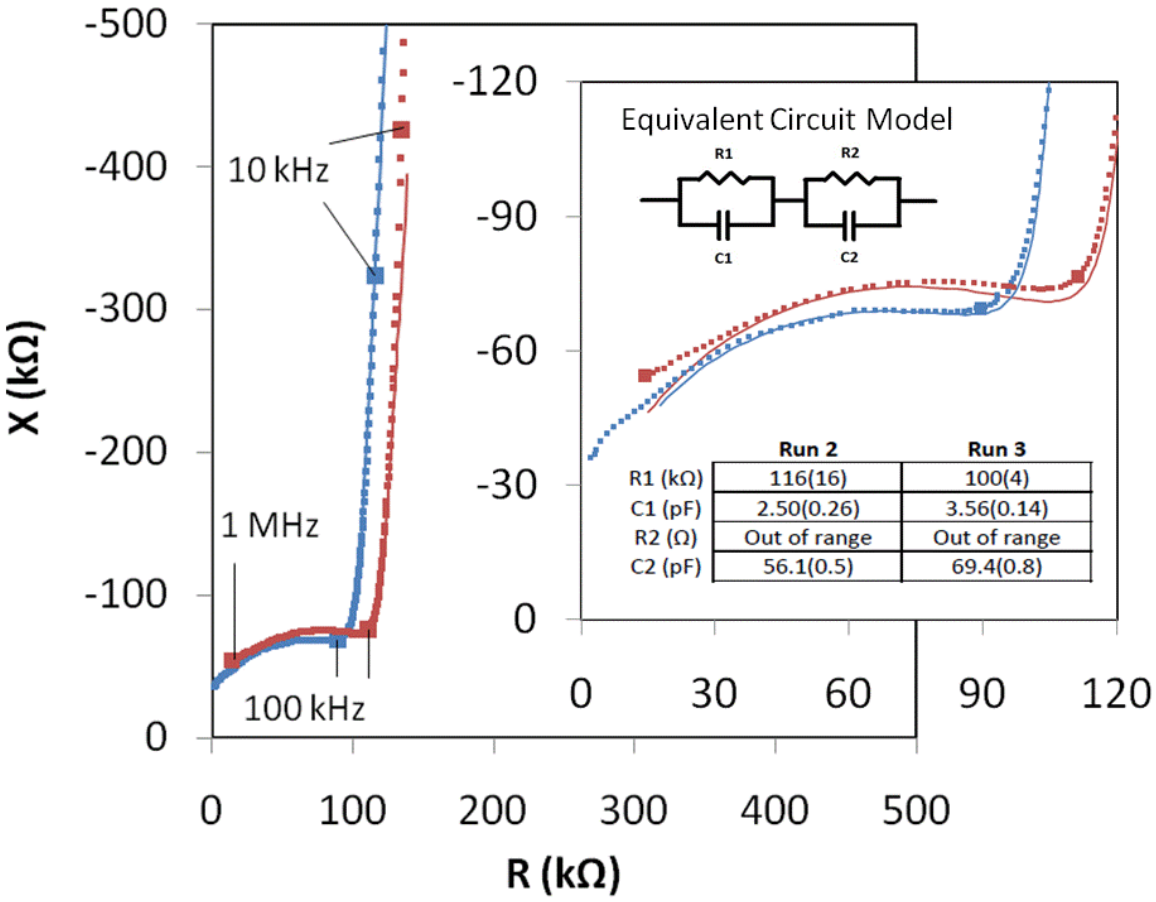

Figure 3 Z spectra of polycrystalline CH_4 hydrate from runs 2 (red) and 3 (blue) with data fits shown as solid lines (corresponding colors) at 4°C, modeled with two parallel R-C pairs in series. Real Z ($R = Z^*\cos(\Theta)$) is plotted versus imaginary Z ($X = Z^*\sin(\Theta)$), where $|Z|^2 = R^2 + X^2$ and $\Theta = \tan^{-1}(X/R)$. Fitting results are tabled in the inset. Z spectra consist of overlapping semicircular arcs. The smaller arcs at high frequency (shown partly as a rapid change in X for R > ~100 kΩ and frequencies < ~100 kHz at 4 °C) resulted from the material properties of the samples (R1, C1; shown in detail in inset). The larger arcs (only partly shown) at low frequency (< ~100 kHz at 4 °C) were caused by electrode polarization (R2, C2). Modeling indicates that σ can be calculated from |Z| corresponding to the smallest value of |Θ| (Modified from Du Frane et al., *In Press, Geophys. Res. Lett.*).

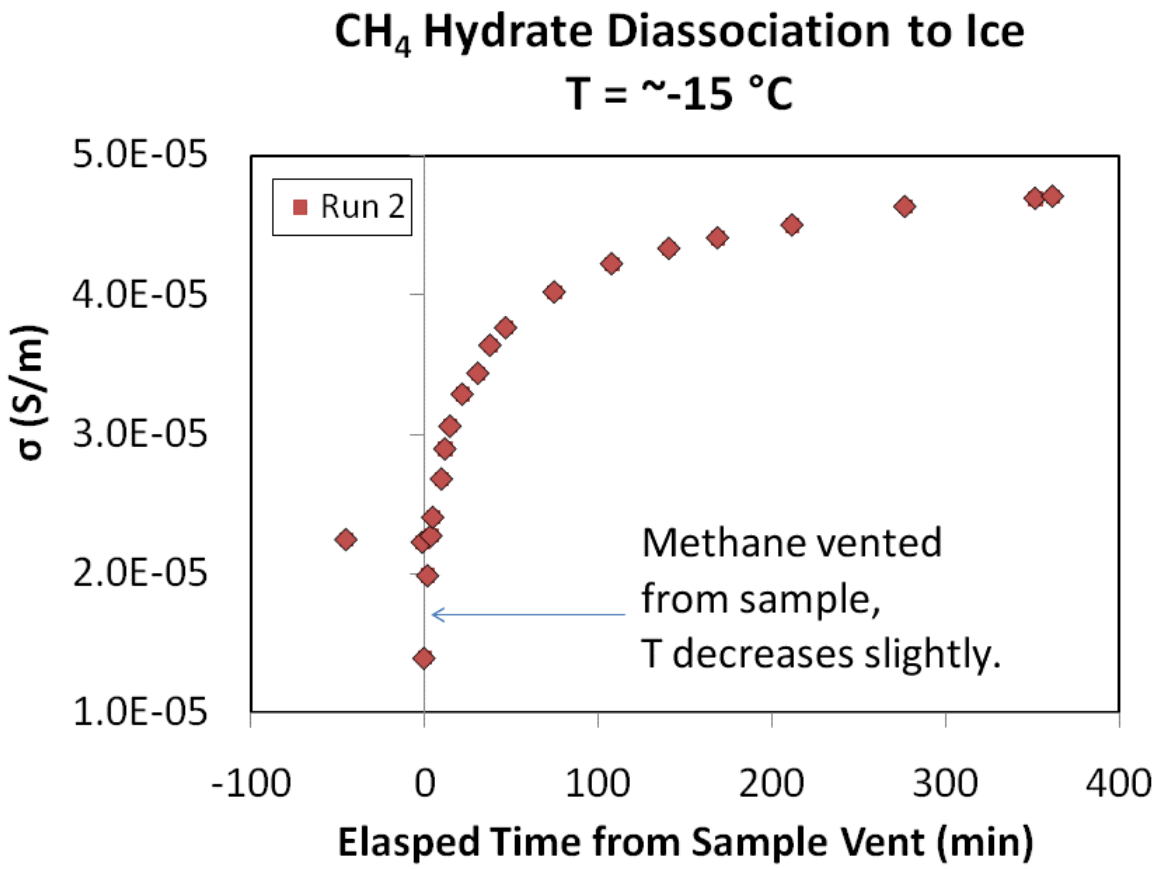

Figure 4 The σ of CH_4 hydrate (run 2) versus time during venting of methane and an initial segment of the subsequent dissociation to ice.

For runs 2 and 3, σ was measured during the initial heating cycle and after CH_4 hydrate was fully synthesized (i.e. after > 6 heating cycles). The samples were then dissociated to polycrystalline ice by venting the pressurized CH_4 from the sample at -15 °C (1 day for run 2, and 13 days for run 3). The σ of the samples increased during dissociation to ice (Figure 4). In both runs, σ of the samples as CH_4 hydrate were a factor of ~3-4 lower than σ of the samples as ice. For both ice and CH_4 hydrate σ exhibited typical Arrhenius behavior (Figure 5). Therefore, we fit the σ data as a function of absolute temperature (T) using

$$\sigma(T) = \sigma_0 \exp\{-E_a/(RT)\} \quad (1)$$

where σ_0 is a pre-exponential constant corresponding to $T = \infty$, and R is the gas constant (fitting results listed in Table 1). Larger error is associated with E_a calculated during active heating because of the variable amount by which the bath temperature lagged sample temperature. We consider the E_a calculated from run 3 using the 'step-dwell' approach to be the more reliable, nevertheless there is good agreement between runs 2 and 3 (Figure 5).

DISCUSSION

Previous experience indicates that most sample transformation to hydrate occurs while passing the melting point of ice during the first heating cycle [29]. Our σ results during the first cycle are consistent with this, assuming that ice dominated the electrical properties of the sample below its melting point, and the small amount of unreacted liquid water dominated above the ice point (Figure 5). Pores within our CH_4 hydrate samples did not have a significant effect on σ due to their lack of connectivity and their being gas-filled, not water-filled [32]. Using the Hashin-Shtrikman mixing model we calculate that σ of nonporous CH_4 hydrate would be a factor of 1.37 (0.137 log units) higher than our measurements for 20% porous gas hydrate.

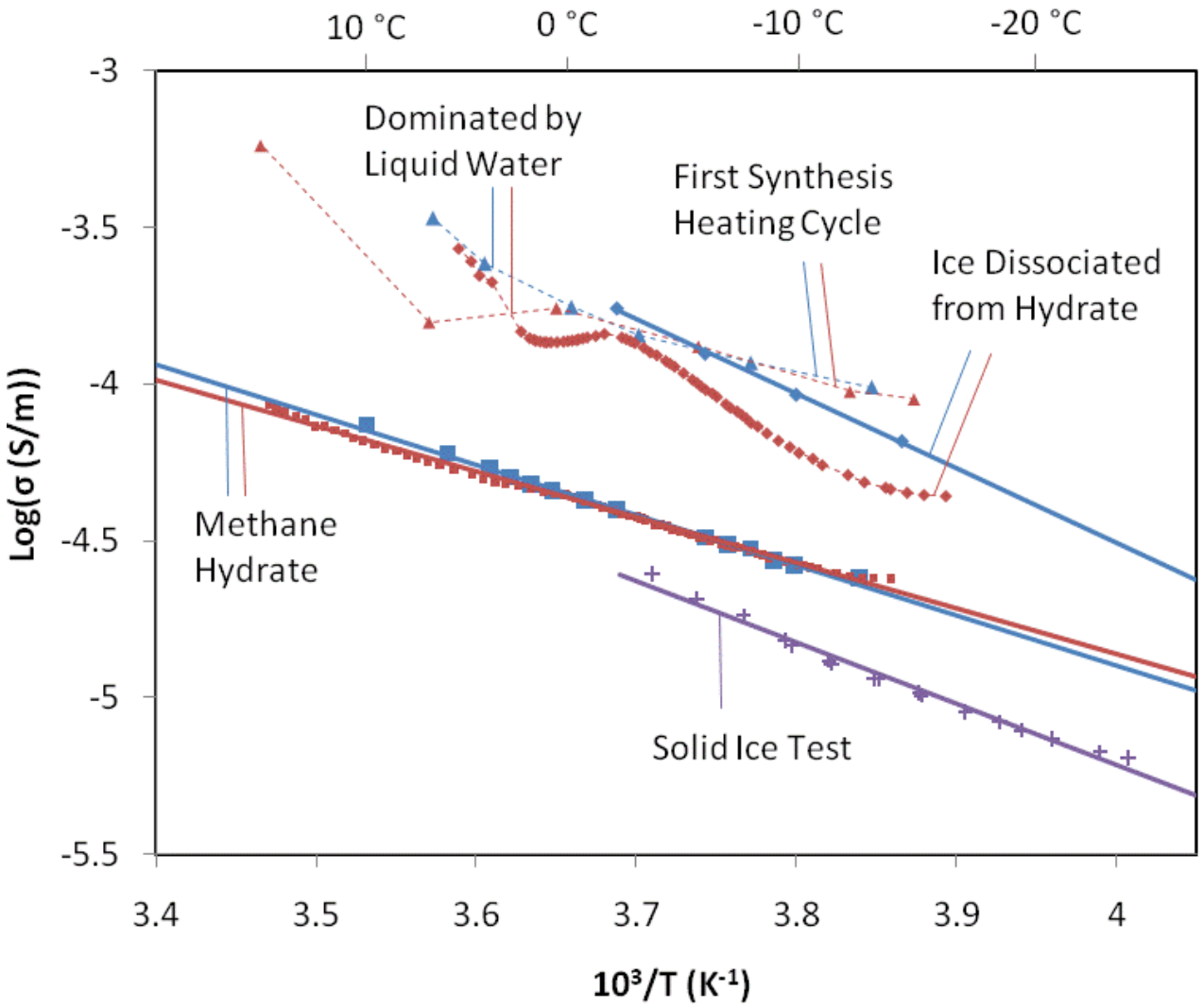

Figure 5 The σ collected during the first heating cycle (triangles), after methane hydrate synthesis (squares), and after dissociation to ice (diamonds), showing the reproducible measurements of runs 2 (red) and 3 (blue); solid ice frozen from reagent grade water (purple plus signs). Data fits are shown as solid lines (corresponding colors). Samples as CH_4 hydrate are 0.5-0.6 log units below values as ice. E_a is ~33% lower for CH_4 hydrate than ice (proportional to the slope of data fits, results in Table 1). Measurements during the first heating cycle after crossing the ice point remain relatively high due to the small amount of unreacted H_2O in grain interiors prior to full reaction to hydrate (Modified from Du Frane et al., *In Press, Geophys. Res. Lett.*).

After several more heating/cooling cycles we do not observe a discontinuity in σ or E_a below or above the melting point of ice, suggesting that samples had fully reacted into CH_4 hydrate. This is consistent with previous observations that all ice reacts within 1-5 heating/cooling cycles, depending in part on the on the grain size and packing density of the initial ice grains [28, 29]. In both runs 2 and 3, synthesis of CH_4 hydrate resulted in lower σ and E_a in our samples compared to the first heating cycle.

After venting the samples, most of the CH_4 hydrate dissociated to ice within several hours; however, the dissociation rates for the last remaining hydrate is complicated by the effects of self preservation or self buffering of the hydrate [33]. For run 2 a small amount of hydrate may have remained in the samples at the center of

grains, in which case this secondary phase would be poorly connected and have little contribution to the measured electrical properties. Run 3 dissociated for a much longer period and likely had no hydrate remaining in the sample when σ was measured. In both runs σ and E_a were lower for CH_4 hydrate than for the dissociated ice product.

The σ of ice is known to be determined by the concentration of intrinsic Bjerrum defects (L and D) and extrinsic protonic defects (H_3O^+ and OH^-) resulting from ionic impurities. There are higher concentrations/mobilities of these defects in grain surfaces where it takes less energy to form than within the bulk grains [e.g., 23]. This is demonstrated by lower σ in ice frozen from reagent grade water (< 1 ppm contaminants) than ice frozen from less pure DDI water used in gas hydrate experiments (Figure 5). Assuming similar defects conduct charge in hydrate suggests the magnitude of σ is also likely to be dependent on impurities. Although we did not characterize the impurity of our samples, the same ionic impurities existed in the bulk samples as either ice or hydrate. Good reproducibility of σ measurements suggests similar concentrations of impurities were in samples from runs 2 and 3.

Lower σ in hydrate than ice is consistent with greater site spacing. Accommodation of a large hydrocarbon molecule in the clathrate structure potentially reduces the site densities of all point defects relative to the ice structure (Ih) which would increase the energy necessary for defects to hop to neighboring sites. This would result in reduced defect mobilities and may explain why both σ (this study) and thermal conductivity [34, 35] are lower for hydrate than ice.

Natural occurrences of gas hydrates comprise of mixtures with sediment and ice or seawater. The σ that we measure for gas hydrate is much less than for seawater (5.6×10^{-1} to 3.8×10^{1} corresponding to salinities between 5 and 40, at 5 °C) [32] and much greater than quartz sand (< ~10^{-18} S/m) [36]. Connectivity of multiphase assemblages is an important factor in determining the σ of mixtures. The presence of a well connected seawater phase would dominate the properties of the mixture, consistent with higher σ measurements of samples mixed with water (~10^{-3}-10^{-2} S/m) in comparison to our σ measurements of unmixed CH_4 hydrate [25-27]. Conversely, high saturations of gas hydrate would dominate mixtures that have little or poorly connected water present; further work is especially needed to resolve mixing relationships for this case. Another potentially important factor in determining the σ of gas hydrate-sediment mixtures is chemical interaction between phases. The presence of fine grained clays and minerals may increase ionic impurities within the gas hydrate phase, which would likely alter the electrical properties of the gas hydrate and overall mixture.

CONCLUSION

We have performed the first electrical measurements of unmixed, polycrystalline CH_4 hydrate (with 20% unconnected intergranular porosity) over the temperature range of -15 to 15 °C; the E_a is 30.6 kJ/mol. We measure σ of CH_4 hydrate at 0 °C to be 5×10^{-5} S/m, which helps to verify that EM surveys may be used to map hydrates in seafloor sediments and provides a more quantitative basis for modeling using mixing laws. Future experiments will be conducted on CH_4 hydrate + sediment aggregates (± seawater) to measure electrical properties of mixed-phase samples.

ACKNOWLEDGEMENTS

The authors thank W. Durham (MIT) and D. Lockner, W. Waite, and S. Kirby (USGS) for helpful discussions and advice and J. Lemire (SIO) for help with the cell fabrication and design. We also thank R. Evans (WHOI) and another anonymous GRL reviewer. Support for this work was provided by DOE contract, DE-NT0005668. Partial support was also provided by Interagency Agreement DE-NT0006147 between the USGS Gas Hydrates Project and the U.S. Department of Energy's Methane Hydrates R&D Program. Prepared by LLNL under Contract DE-AC52-07NA27344. Modified from a manuscript accepted for publication in Geophysical Research Letters.

REFERENCES

[1] Kvenvolden KA. *Potential effects of gas hydrate on human welfare*. Proc. Natl. Acad. Sci. U. S. A. 1999;96(7):3420-3426.

[2] Shakhova N, Semiletov I, Salyuk A, Yusupov V, Kosmach D, and Gustafsson O. *Extensive Methane Venting to the Atmosphere from Sediments of the East Siberian Arctic Shelf.* Science 2010;327(5970):1246-1250.

[3] Maslin M, Owen M, Betts R, Day S, Dunkley Jones T, and Ridgwell A. *Gas hydrates: past and future geohazard?* Proc. R. Soc. A 2010;368(1919):2369-2393.

[4] Mienert J, Vanneste M, Bunz S, Andreassen K, Haflidason H, and Sejrup HP. *Ocean warming and gas hydrate stability on the mid-Norwegian margin at the Storegga Slide*. Mar. Pet. Geol. 2005;22(1-2):233-244.

[5] Nixon MF, and Grozic JLH. *Submarine slope failure due to gas hydrate dissociation: a preliminary quantification*. Can. Geotech. J. 2007;44(3):314-325.

[6] Dawe RA, and Thomas S. *A large potential methane source - Natural gas hydrates*. Energy Sources Part A-Recovery Util. Environ. Eff. 2007;29(3):217-229.

[7] Hovland M, and Gudmestad OT. *Potential influence of gas hydrates on seabed installations*. In: Paull CK and Dillon WP, editors. Natural Gas Hydrate Occurrence, Distribution, and Detection, Geophys. Mongr. Ser. 2001. pp. 307-315, AGU, Washington D. C.

[8] Kvenvolden KA. *Gas hydrate and humans.* Ann. N. Y. Acad. Sci. 2000;912: 17–22, doi: 10.1111/j.1749-6632.2000.tb06755.x.

[9] Milkov AV. *Global estimates of hydrate-bound gas in marine sediments: how much is really out there?* Earth-Sci. Rev. 2004;66(3-4):183-197.

[10] Archer D and Buffett B. *Time-dependent response of the global ocean clathrate reservoir to climatic and anthropogenic forcing*. Geochem., Geophys., Geosystems 2005;6:1-13.

[11] Klauda JB, and Sandler SI. *Global distribution of methane hydrate in ocean sediment*, Energy Fuels, 2005;19(2):459-470.

[12] Boswell R, and Collett T. *Current perspectives on gas hydrate resources*. Energy Environ. Sci. 2010;4:1206-1215, DOI: 10.1039/C0EE00203H, Perspective.

[13] Hornbach MJ, Holbrook WS, Gorman AR, Hackwith KL, Lizarralde D, and Pecher I. *Direct seismic detection of methane hydrate on the Blake Ridge*. Geophysics 2003;68(1):92-100.

[14] Dai J, Banik N, Gillespie D, Koesoemadinata, A, Dutta N. *Exploration for gas hydrates in the deepwater, northern Gulf of Mexico: Part II. Model validation by drilling*. Marine Petrol. Geol. 2008;25:845-859.

[15] Dai J, Snyder F, Gillespie D, Koesoemadinata A, Dutta N. *Exploration for gas hydrates in the deepwater, northern Gulf of Mexico: Part I. A seismic approach based on geologic model, inversion, and rock physics principles*. Marine Petrol. Geol., 2008;25:830-840.

[16] Zhang ZJ, and McMechan GA. *Elastic inversion for distribution of gas hydrate, with emphasis on structural controls*. J. Seismic Explor. 2006;14(4):349-370.

[17] Collett TS and Ladd JW. *Detection of gas hydrate with downhole logs and assessment of gas hydrate concentrations (saturations) and gas volumes on the Blake Ridge with electrical resistivity log data*. Proc. Ocean Drill. Program, Sci. Results 2000;164:179-191.

[18] Edwards RN. *On the resource evaluation of marine gas hydrate deposits using sea-floor transient electric dipole-dipole methods*. Geophysics 1997;62(1):63-74.

[19] Evans RL. *Using CSEM techniques to map the shallow section of seafloor: From the coastline to the edges of the continental slope.* Geophysics 2007;72(2):WA105-WA116.

[20] Schwalenberg K, Willoughby E, Mir R, and Edwards RN. *Marine gas hydrate electromagnetic signatures in Cascadia and their correlation with seismic blank zones*. First Break 2005;23:57-63.

[21] Weitemeyer KA, Constable S, and Key KW. *Marine EM techniques for gas-hydrate detection and hazard mitigation.* The Leading Edge 2006a;25:629-632.

[22] Weitemeyer KA, Constable S, Key KW, and Behrens JP. *First results from a marine controlled-source electromagnetic survey to detect gas hydrates offshore Oregon.* Geophys. Res. Lett. 2006b;33(3):L03304,doi:10.1029/2005GL024896.

[23] Petrenko VF, and Whitworth RW. *Physics of Ice*. Oxford Univ. Press Inc., New York. 1999.

[24] Zhou X, Fan S, Liang D, Wang D, and Huang N. *Use of electrical resistance to detect the formation and decomposition of methane hydrate.* J. Natural Gas Chem. 2007;16:399-403.

[25] Spangenberg E, and Kulenkampff J. *Influence of methane hydrate content on electrical sediment properties*. Geophys. Res. Lett. 2006;33(24).

[26] Lee JY, Santamarina JC, and Ruppel C. *Parametric study of the physical properties of hydrate-bearing sand, silt, and clay sediments: 1.*

Electromagnetic properties. J. Geophys. Res. 2010;115:B11104, doi:10.1029/2009JB006669.
[27] Ren SR, Liu Y, and Zhang W. *Acoustic velocity and electrical resistance of hydrate bearing sediments*. J. Petrol. Sci. and Engineer. 2010;70:52-56.
[28] Stern LA, Kirby SH, and Durham WB. *Peculiarities of methane clathrate hydrate formation and solid-state deformation, including possible superheating of water ice.* Science 1996;273(5283):1843-1848.
[29] Stern LA, Kirby SH, Circone S, and Durham WB. *Scanning electron microscopy investigations of laboratory-grown gas clathrate hydrates formed from melting ice, and comparison to natural hydrates.* Am. Mineral. 2004;89(8-9):1162-1175.
[30] Roberts JJ, and Tyburczy JA. *Impedance spectroscopy of single and polycrystalline olivine - evidence for grain-boundary transport*. Phys. Chem. Miner. 1993;20(1):19-26.
[31] Roberts JJ, and Tyburczy JA. *Frequency-dependent eletrical-properties of polycrystalline olivine compacts.* J. Geophys. Res., [Solid Earth], 1991;96(B10):16205-16222.
[32] *CRC Handbook of Chemistry and Physics.* 91st ed. CRC Press: Boca Raton, FL. 2010.
[33] Stern LA, Circone S, Kirby SH, and Durham WB. *Anomalous preservation of pure methane hydrate at 1 atm*. J. Phys. Chem. B, 2001;105(9);1756-1762.
[34] deMartin BJ. *Laboratory measurement of the thermal conductivity and thermal diffusivity of methane hydrate at simulated in-situ conditions*. M.S. Thesis, Sch. Earth Atmos. Sci., Georgia Inst. Tech., Atlanta, GA. 2001.
[35] Waite WF, Stern LA, Kirby SH, Winters WJ, and Mason DH. *Simultaneous determination of thermal conductivity, thermal diffusivity and specific heat in sI methane hydrate*. Geophysical J. Int., 2007;169(2):767-774.
[36] Serway RA. *Principles of Physics.* 2nd Ed. Fort Worth, Texas; London: Saunders College Pub. p. 602. 1998.